Journal of Advanced Scientific Research

Available online through http://www.sciensage.info

ISSN 0976-9595

Research Article

# PREPARATION OF $La_{1-X}Nd_XCoO_3$ SYSTEM FOR MATERIALS AND CATALYTIC CO OXIDATION STUDIES

**Teotone Vaz*[1], S. M. Gurav[2], A. V. Salker[3]**

[1]*St. Xavier's College, Mapusa, Goa, India*

[2]*Govt. College of Arts, Sc., and Com, Quepem, Goa, India*

[3]*School of Chemistry, Goa University, Goa, India*

**Corresponding author: teovaz18@gmail.com*

**ABSTRACT**

Crystalline Lanthanum and Neodymium Cobaltates with a perovskite structure $ABO_3$ and their intermediate compositions $La_{1-X}Nd_XCoO_3$ (x = 0.0, 0.3, 0.5, 0.7 and 1.0) were successfully prepared via co-precipitation precursor technique as low as at 800°C temperatures. The crystal structure and their phase formation were confirmed by X- ray powdered diffraction. The terminal compounds $LaCoO_3$ and $NdCoO_3$ were identified to be single phase and are indexed to Rhombohedral and Orthorhombic structures respectively. The intermediate x=0.3, and 0.5 show Rhombohedral whereas x = 0.7 is indexed to Orthorhombic structure. The bonding characteristics were studied by FTIR spectroscopy. TGA/DSC technique reveals the optimum calcination temperature for the formation of perovskite phase. Magnetic susceptibility measurements and ESR study provide an insight into the paramagnetic catalytically active species. An attempt has been made to understand the effect of A-site substitution in the lattice of $LaCoO_3$ with $Nd^{+3}$ ions and their correlation with the solid-state properties. Being thermally stable materials, they were tested for a model catalytic CO oxidation for pollution control strategy. They showed an increase in the activity of carbon monoxide oxidation to carbon dioxide.

**Keywords:** Rare earth cobaltite, Co-precipitation precursor, Solid state studies, Carbon monoxide oxidation.

## 1. INTRODUCTION

The perovskite type rare earth Cobalt oxides $ACoO_3$ (A=Lanthanide ion) present very interesting physical properties including magnetic phase and structural transitions. They exhibit a variety of applications in microelectronics, cathods in solid oxide fuel cells (SOFC), oxygen separation mem-branes, electro-ceramics and refractory materials, sensor materials, magnetic memory devices and as catalysts, due to their stability in thermal and chemical atmospheres [1-6]. The $Ln^{+3}$ ions support the framework, stabilizes the system and hence the size of these ions defines the octahedral structural transformations. Their properties are influenced by the ionic radius of $Ln^{+3}$, mainly due to bond length induced structural distortions which in turn not only affect the crystal structure but governs the electronic state and decides the physical properties [6]. It has been known that a particular synthetic route influences the physical changes in the volume and surface properties of the material, for example, its structure, morphology, porosity, and particle size [7, 8]. Nowadays, various synthesis methods are investigated in order to achieve control of the shape and size of the materials in nano range. Several researchers have synthesized $LaCoO_3$ and $NdCoO_3$ poly-crystalline materials comparatively in pure form either by modified conventional ceramic, co-precipitation, sol-gel, hydrothermal, auto-combustion and also by other modern techniques like pulse laser, spray pyrolysis techniques for thin films. $LaCoO_3$ is largely found in Rhombohedral, whereas $NdCoO_3$ was reported to be obtained in Cubic and Orthorhombic crystal structure material [8-12].

The rare earth-transition metal perovskite oxides provide an excellent base for correlating catalytic and solid state properties because they can be well characterized by different techniques [13]. Monitoring the environment for hazardous chemicals is of great concern to save our surrounding clean and

safe. These compounds are considered as active catalyst materials replacing noble metals particularly for environmental catalysis like treatment of exhaust gases and oxidation of carbon monoxide (CO). The catalytic activity of these perovskites can be suitably modified by incorporating different metal ions in the lattice to improve the quality of materials. The oxidation of CO with the aim of reducing air pollutant is obviously an important model reaction to check the efficacy of perovskite materials as catalyst [5, 14-16].

In this investigation, we present an understanding of the effect of A-site progressive substitution of Nd in the lattice of $LaCoO_3$ on their physical properties prepared by co-precipitation precursor technique and their correlation with the spectroscopic and solid state properties. Also, these compositions are known for their stability at higher temperatures, we explore their potential as candidates for Carbon monoxide (CO) conversion, as model test reaction.

## 2. MATERIAL AND METHODS

### 2.1. Co-precipitation precursor synthesis

The perovskite type $La_{1-X}Nd_XCoO_3$ (x = 0.0, 0.3, 0.5, 0.7 and 1.0) compositions were synthesized by co-precipitation precursor technique using NaOH solution as discussed earlier [16, 17]. Stoichiometric quantities of hydrated $La(NO_3)_3$, and or $Nd_2O_3$, $Co(NO_3)_3$ (AR) were dissolved in 100mL of pure water and /or $Nd_2O_3$ was dissolved in minimum quantity of 1:1 Nitric acid. Both solutions were mixed on magnetic stirrer and precipitated using 5% sodium hydroxide solution. The resultant precursor hydroxide precipitate was digested and the mixture was subjected to oxidation using 6% $H_2O_2$. The precipitate was then washed, filtered and dried in an oven at 120°C. The dried precipitate was homogenized well in an agate mortar and further heated in stages at 300, 600 and finally 800°C in air for a total time of 10-12 hrs. The furnace cooled samples were stored in airtight containers for further studies.

### 2.2. Materials Characterization

The prepared compositions were characterized by X- ray powder diffraction (XRD) technique with Rigaku Miniflex bench top instrument, using Cu Kα, filtered through Ni absorber. Fourier Transformed Infra Red (FTIR) spectra were recorded on a Shimadzu (Model 8101A) instrument. The sodium contamination in the prepared compound was found by employing atomic absorption spectroscopy (AAS). Thermal Gravimetric Analysis (TGA)/ Differencial Scanning Calorimetry (DSC) was carried out using NETZSCH - Garetebau GmbH Thermal Analyzer. The total BET surface areas were measured using BET Nitrogen adsorption method (QUANTACHROME NOVA 1200 version 3.70). Electrical conductivity measurements were carried out by two-probe conductivity cell in the temperature range of room temperature (R.T.) to 525°C. The magnetic susceptibility '$\chi_g$' in air were determined by Gouy method at room temperature employing a field of the order of 10,000 gauss and using Hg [$Co(SCN)_4$] as standard materials. ESR study was carried out for the perovskites containing paramagnetic species and for the identification of the catalytically active species for the reaction. The ESR spectra were recorded at the X- band on a Varian E-112 spectrophotometer at liquid Nitrogen temperature. The sample was mounted on a quartz tube and TCNE was used as a field calibrant taking its g-value as 2.00277. The saturation magnetization was studied considering the hysteresis behaviour. These measurements were done on selected magnetic samples, using a high field hysteresis loop tracer. The saturation magnetization values, σs in emu/g, of these magnetic perovskite samples were measured.

### 2.3. Catalytic CO oxidation as model test reaction

Perovskite materials are well known candidates for catalytic oxidation reactions. So, the prepared compositions were tested for a model reaction of catalytic CO oxidation, using oxygen in Nitrogen with a continuous flow, fixed bed quartz reactor by placing 1.0 g of powdered catalyst in between glass wool plugs. The catalyst activity was determined using a feed gas composition of 5% CO, 5% $O_2$ in Nitrogen for CO oxidation. The feed gases and the products were analyzed employing an online gas chromatograph with a molecular sieve 13X and Porapak Q columns. $H_2$ was used as a carrier gas. The CO was prepared in the laboratory by standard procedures, further purified by passing through alkali and molecular sieve traps [16]. The oxygen and Nitrogen gases were used from pure commercial cylinders.

## 3. RESULTS AND DISCUSSION

### 3.1. Phase formation check by XRD

The prepared materials were characterized by X- ray powder diffractograms. The $d_{hkl}$ and 2θ values obtained were compared with the reported values in the literature and found to be in good agreement. As the literature of the intermediate x=0.3, 0.5 and 0.7 compositions for the $d_{hkl}$ value are not reported, the values were compared with the end compositions. Fig. 1 show XRD pattern for the $La_{1-x}Nd_x CoO_3$ system. Our results of X-ray analysis showed that $LaCoO_3$ x = 0.3 and 0.5 composition could be clearly indexed to rhombohedral (JCPDS data file 34-1181). The diffraction pattern of x= 0.7 and $NdCoO_3$ compounds are indexed to the orthorhombic structure, in accordance with other published work [10, 17]. The rhombohedral distortion of the $LaCoO_3$ perovskite structure was the evidence of the observed characteristic splitting in the diffraction peaks [18]. The crystallite size was calculated using Debye-Scherrer formula from the avarage of four intense peaks, which estimates the size of smaller crystals from their diffraction peaks and found to be in the range of 18.9 to 41.2 nm lowest being for $La_{0.3}Nd_{0.7}CoO_3$ and highest for $LaCoO_3$.

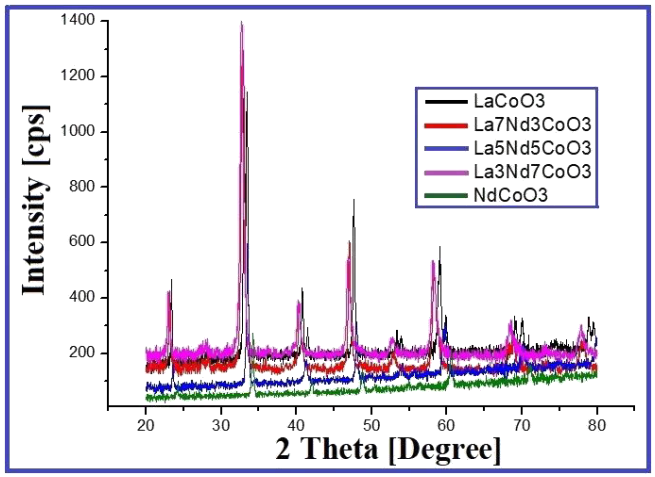


**Fig. 1: XRD patterns for the $La_{1-x}Nd_xCoO_3$ nanomaterials system**

### 3.2. Thermo-gravimetric analysis

TGA was recorded to study the behaviour of weight loss of the precursor samples. A selected precursor (approx. 20mg) was placed in alumina crucible, was continuously weighed as it is heated at a constant linear rate 10°C $min^{-1}$, from R.T. to 900°C. The thermal event exothermic or endothermic proceeding the physical and chemical changes were studied by DSC. Fig. 2, shows a typical TGA and DSC curves for a representative $La_{0.5}Nd_{0.5}Co(OH)_6.xH_2O$ precursor, are in agreement with the combined thermal behaviours respective hydroxides. The weight loss of 11.54% between R.T. to 300°C, due to the loss of moisture, between 325-390°C due to decomposition of hydroxides and further linear weight loss is due to initiation of solid-state diffusion with the together weight loss of 17.52% and perovskite phase formation between 425-850°C.

### 3.3. AAS techniques

As NaOH solution was used for co-precipitation to form the precursor mixture of hydrated $La(OH)_3$ and $Co(OH)_3$, the presence of trace amounts of Na contamination was expected. It was estimated using an AAS and found to be in the range of 0.2 to 0.4 % by weight. Surface areas obtained by BET Nitrogen adsorption method were found to be in the range of 4.3 - 5.8 $m^2/g$.

### 3.4. Perovskite characteristic absorptions by FTIR:

The perovskite compounds are known to be characterized by IR spectra in the region 1000 to 300 $cm^{-1}$. The two strong absorption bands were observed in the 700 to 390$cm^{-1}$ region corresponding to the stretching vibration of metal-oxygen bond. The lower frequency band has been assigned to a deformation mode of $CoO_6$ octahedral. *i.e.* the Co-O-Co bond angles of the perovskite structure. The frequency of these bands has been related to the strength of metal-oxygen covalency.

The FTIR of $LaCoO_3$ compound shows a broad absorption shouldered bands at 600 $cm^{-1}$ and 570 $cm^{-1}$ gradually becomes sharp and no band is observed at 600 $cm^{-1}$, with the substitution of $Nd^{+3}$ in the lattice . Secondly, the low frequency band at 420 $cm^{-1}$ for $LaCoO_3$, keep shifting with the increase in x value and is observed at 471 $cm^{-1}$ for $NdCoO_3$. As the $Nd^{+3}$ ions increases at A-site in the lattice of $LaCoO_3$, the relative distance of $d_{Co-O}$ and $d_{R-O}$ (R=La or Nd) changes, deforming the $CoO_6^-$ octahedra, which gets tilted on account of the atomic size difference [19]. Thus, the relative distance of Co-O and La-O/Nd-O changes, hence the absorption frequency of vibration modes decreases. This may be the probable reason for the observed vibration bands for the spectra b, c, d and e as seen in fig. 3.

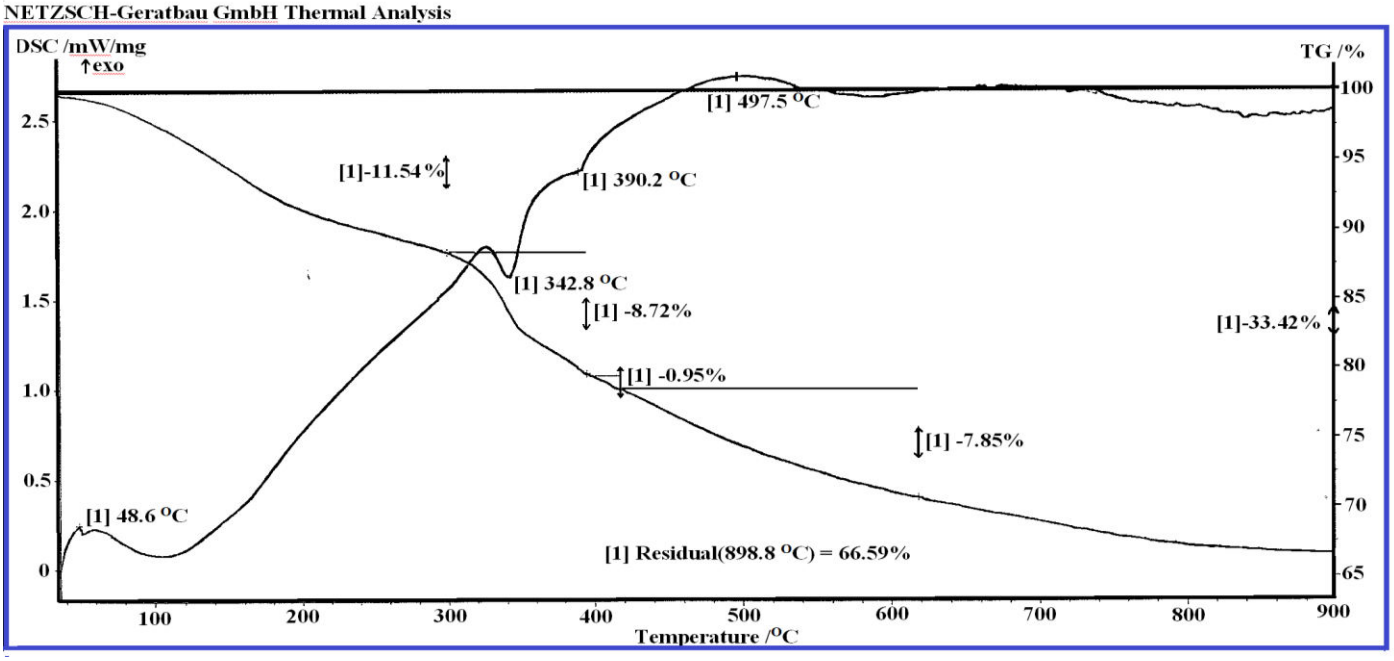


**Fig. 2: Typical TGA and DSC curves for $La_{0.5}Nd_{0.5}Co(OH)_6.xH_2O$ precursor**

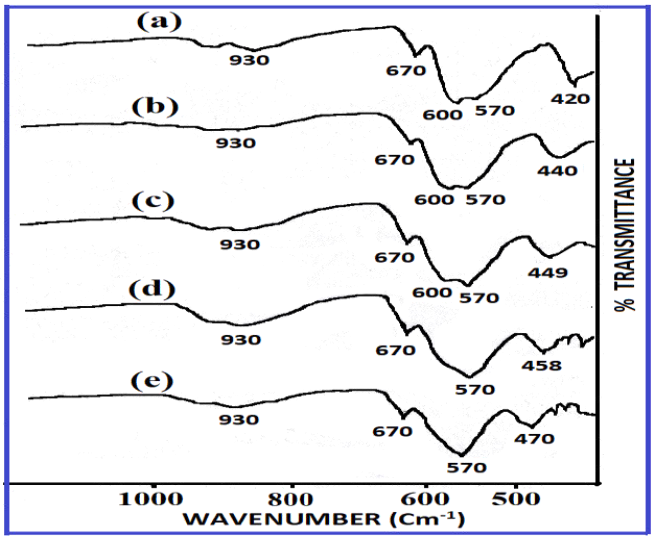


**Fig. 3: FTIR absorption bands of a) $LaCoO_3$, b) $La_{0.7}Nd_{0.3}CoO_3$ c) $La_{0.5}Nd_{0.5}CoO_3$ d) $La_{0.3}Nd_{0.7}CoO_3$, and e) $NdCoO_3$**

### 3.5. Electrical behaviour of nanomaterials

Fig. 4 Shows the trend of temperature dependence of resistivity for R.T. to 525°C. It is seen that the resistivity decreases with increase in the temperature and all compositions show more or less similar resistivity behaviour. For the terminal $LaCoO_3$ and $NdCoO_3$ and mid composition $La_{0.5}Nd_{0.5}CoO_3$ materials, the resistivity decreases in the range from r. t. to 200°C, followed by a broad jump of resistivity in the range of 200°C to 400°C. For further rise in temperature beyond 400°C, a very small change in resistivity was observed. The resistivity curves shows the extrinsic to intrinsic behaviour, typical of the semiconductor materials. There is no phase transition in this compound above R.T. Intermediate compositions x = 0.3 and 0.7 show similar trends but higher resistivity behaviour in the same temperature range.

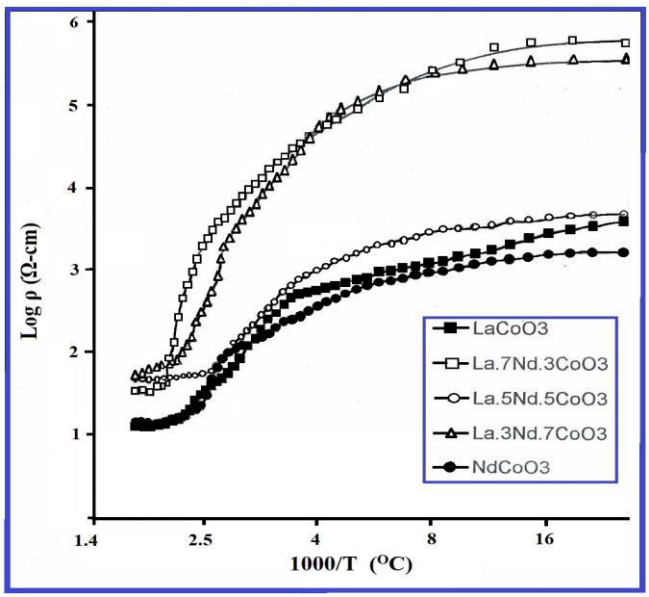


**Fig. 4: Variation of electrical resitivity of $La_xNd_{1-x}CoO_3$ system**

### 3.6. Magnetic behaviour

The magnetic susceptibility behaviour was investigated for their paramagnetic nature by Gouy balance at R.T. using field strength of 10,000 gauss. The observed gram susceptibility and the saturation magnetization values are presented in table 1. The gram susceptibility value for $LaCoO_3$ was 1.96 x $10^{-5}$, which goes on increasing with the substitution with $Nd^{+3}$ ions to 2.85 x $10^{-5}$ emu/g for $NdCoO_3$. Similarly, a gradual increase of $\mu_{eff}$ was observed from 3.4 to 4.16 B.M. In $La_{1-x}Nd_xCoO_3$ nano-system, as x value increases, there is a gradual change in the symmetry from rhombohedral to orthorhombic structure, which gets reflected in their magnetic susceptibility values. This explains the higher magnetic susceptibility for orthorhombic $NdCoO_3$ and lower value for $LaCoO_3$ having rhombohedral structure.

**Table 1: Crystallite size, Specific surface area, Gram susceptibility ($\chi_g$), Magnetic moment ($\mu_{eff}$), Saturation magnetization and ESR data of nanomaterials**

| Compound | Crystallite size (nm) | Surface Area ($M^2/g$) | $\chi_g$ at r. t. (emu/g) g-value (emu/g) (80 K) | $\mu_{eff}$ (B.M.) | g-value (80 K) | Line Width (gauss) |
|---|---|---|---|---|---|---|
| $LaCoO_3$ | 41 | 5.4 | 1.90 x $10^{-5}$ | 3.40 | 3.7 | 940 |
| $La_{0.7}Nd_{0.3}CoO_3$ | 24 | 4.3 | 2.23 x $10^{-5}$ | 3.65 | - | - |
| $La_{0.5}Nd_{0.5}CoO_3$ | 34 | 5.8 | 2.46 x $10^{-5}$ | 3.85 | 7.5 | 1020 |
| $La_{0.3}Nd_{0.7}CoO_3$ | 19 | 5.7 | 2.68 x $10^{-5}$ | 4.00 | - | - |
| $NdCoO_3$ | 27 | 4.9 | 2.85 x $10^{-5}$ | 4.16 | 7.4 | 1180 |

### 3.7. ESR studies

ESR studies were carried out, to get an insight about the catalytically active, paramagnetic species and used as qualitative tool to ascertain the changes occurring with the A-site substitution of $La^{+3}$ with $Nd^{+3}$ ions in their $LaCoO_3$ lattice structures. The nanocatalyst materials showed Lorentzian-shaped ESR lines at liquid nitrogen temperature. Fig. 5 illustrates the ESR spectra and the data obtained at liquid nitrogen temperature are presented in table 1. No signal at R.T. and a very weak ESR signal with broad line width was observed for $LaCoO_3$ material with g-value 3.7 at liquid nitrogen($N_2$), indicating that $La^{+3}$ and $Co^{+3}$ ions are ESR inactive. It is clearly visible that the g-value of $La_{1-X}Nd_XCoO_3$ nanosystem was found to increase with increasing 'x' value,for x = 0.5 with g-value of 7.5, which becomes sharp for fully substituted $NdCoO_3$ compound with corresponding g-value of 7.4.

For heavier atoms like $La^{+3}$ions, the spin-orbit coupling is strongly coupled to lattice vibrations and spin relaxation time, therefore, it is very small at high temperatures. This means that ESR spectra too broad to be detected at R.T. The broad line spectra observed at liquid nitrogen temperature was due to the presence of paramagnetic $Nd^{+3}$ ions having a nuclear moment and a short lifetime of the excited state. Thus, the line width depends on the relaxation time of the spin state through either or both of the processes spin-lattice and spin-spin relaxation. The interaction of paramagnetic ions with the thermal vibrations of the lattice leads to short spin-lattice relaxation time. At low temperature, the spin-lattice relaxation becomes less efficient, as the violence in the inter-atomic motion decreases, thus increasing the relaxation time [20].

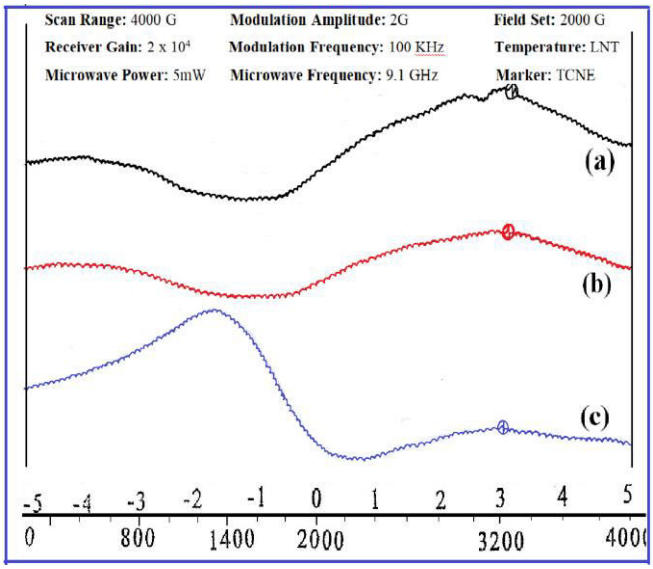


**Fig. 5: ESR spectra of selected a) $LaCoO_3$, b) $La_{0.5}Nd_{0.5}CoO_3$ and c) $NdCoO_3$**

### 3.8. SEM analysis

Fig. 6 show representative SEM images of $La_{1-X}Nd_X CoO_3$ nanoperovskite materials, with 80.00 KX magnifications. In all the images, particles with semi to spherical shapes can be observed. In all the micrograph images a clear spherical-shaped granular nanoparticles agglomeration was prominent. The significant morphological clarity are observed due to oxyphilic nature of Co atoms, promoting the formation of better spherical shaped particles having higher porosity. Overall, the observed morphology was the result of the agglomeration of very small polycrystalline particles in nano range.

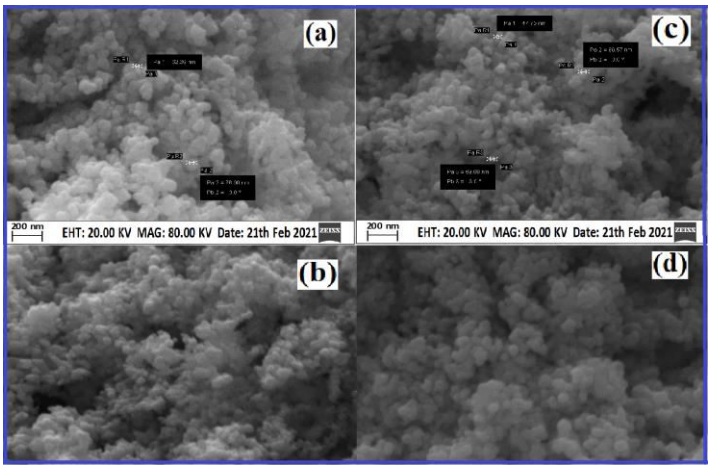


**Fig. 6: SEM image of a) $LaCoO_3$, b) $La_{0.5}Nd_{0.5}CoO_3$, c) $La_{0.3}Nd_{0.7}CoO_3$, and d) $NdCoO_3$ polycrystalline nanoparticles**

### 3.9. Catalytic CO oxidation as model test reaction

The rare earth - transition metal perovskites provide an excellent base for correlating catalytic and solid state properties, because such materials can be easily characterized by different techniques. So, the prepared materials were tested for a model reaction of catalytic CO oxidation resembling environmental pollution. The surface areas of prepared compositions were measured by BET Nitrogen adsorption at boiling liquid Nitrogen temperatures, employing high speed gas sorption analyser. The surface area were comparatively less and in the range of 4.3 to 5.8 $m^2/g$. The low surface areas of these compositions may be due to sintering.

The temperature dependence of CO conversion studies for different compositions of $La_{1-X}Nd_XCoO_3$ materials system is shown in fig. 7. The rate of CO oxidation gradually increases with the increased substitution of $Nd^{+3}$ ions in the $LaCoO_3$ lattice. For the compositions x = 0.0, 0.3 and 0.5, showed marginal increase and achieving higher oxidation efficiency with the temperature. It may be noted that all materials show 100% catalytic efficiency with $NdCoO_3$ and $LaCoO_3$ at lower temperature of 175°C and higher at 225°C. The $La_{0.7}Nd_{0.3}CoO_3$ compound exhibited a lesser CO oxidation efficiency. The induction temperature for x = 0.3 and $LaCoO_3$ compound was higher but they also show reasonable efficiency at 225°C. The specific surface area of these materials does not appear to be the criteria for the displayed trend of catalytic activity, as all the materials possess more or less similar surface area. In fact, $NdCoO_3$ showing highest efficiency, indeed possess surface area lower than $LaCoO_3$ material. $ABO_3$ perovskites, in which the A = Lanthanide ions are essentially inactive in catalysis and B- site active transition metal ions are placed at relatively large distances from each other are excellent catalytic models for the study of interactions of CO and $O_2$ on single surface site. Studies have shown that among non-metal metal containing catalysts $Co^+$ ions are chemically active for CO oxidation. Since in our study, B- site Cobalt metal, being present in the same amount in all the compositions, the observed differences in catalytic activity needs to be explained with respect to increase substitution in the A- site by $Nd^{+3}$ ions and its effect on $LaCoO_3$ crystal structure. The catalytic activity for the CO oxidation is closely related to the electronic structure of the surface oxide ions [13].

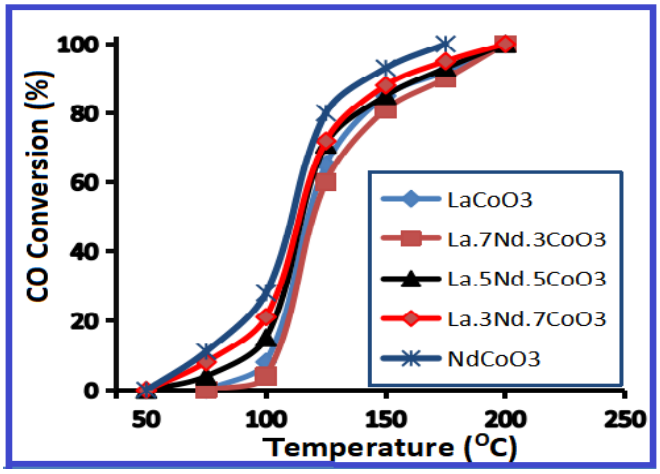


**Fig. 7: Catalytic CO oxidation efficiency on $La_xNd_{1-x}CoO_3$ system**

The enhancement of catalytic oxidation capacity with the substitution of $Nd^{+3}$ ions in the $LaCoO_3$ lattice structure can be explained on A-site ionic size effect. Smaller the A-site rare earth ion, higher is the catalytic activity, which is correlated to the surface oxygen binding energy [21, 22]. $LaCoO_3$ having a distorted rhombohedral structure with optimized Co-O bond length having the large size $La^{+3}$ ions occupies 12 - coordinated A- site while, $NdCoO_3$ an orthorhombic structure. The catalytic oxidation properties are sensitive to the $La^{+3}$ and $Nd^{+3}$ ions at A-site, mainly due to the structural distortion induced by the La-O, Nd-O and Co-O bond lengths. These distortions besides affecting the crystal structure also influence physical properties including catalytic activity. With the increased substitution of $La^{+3}$with the $Nd^{+3}$ ions at A-site in the $LaCoO_3$ lattice, A- site ionic radii decreases, effecting the Co-O bond lengths, which has direct impact on the surface lattice oxygen binding energy. In the case of $LaCoO_3$ nano material, the binding is comparatively stronger *i.e.* the interactions of Co-O-Co bond strength, which hinders the release of lattice oxygen at the surface of the catalyst and the creation of oxygen vacancies at the surface. Since CO is reducing gas, having tendency to reduce the lattice oxygen from the catalyst surface creating oxygen vacancies, which is later filled by oxygen supplied during the catalytic reaction. Thus, higher binding energy for the surface oxygen species is comparatively unfavorable for the $LaCoO_3$ material to be active for CO Oxidation. As $La^{+3}$ ions are increasingly substituted by $Nd^{+3}$ ions in the lattice of $LaCoO_3$, due to substituted $Nd^{+3}$ion size difference, resulting in the variation in Nd-O and Co-O bond lengths, impact on the lower binding energy of surface lattice oxygen. As a result, there is an enhancement in the formation of oxygen vacancies at the surface of lattice, which may be a probable reason for enhancement in the CO oxidation capacity of $NdCoO_3$ [13, 22].

## 4. CONCLUSION

Crystalline $LaCoO_3$ and $NdCoO_3$ perovskite nano-materials and their selected intermediates were successfully prepared by stabilizing Co(III) state with $H_2O_2$ by a comparatively low temperature synthetic method. Systematic $La^{+3}$substitution by $Nd^{+3}$ ions in the $LaCoO_3$ lattice and their impact on structural, morphological changes, electrical resistivity, magnetic properties and catalytic CO oxidation as model test reaction are the highlights of this investigation. A significant increase in the catalytic efficiency was observed with the gradual A-site substitution. All the nanoperovskite materials show 100 % oxidation efficiency in the temperature range of 175 to 225°C. Binding energy of the surface lattice oxygen on these materials plays a crucial role in the catalytic efficiency. In comparison, $NdCoO_3$ nanomaterial show the higher activity than $LaCoO_3$, due to its lower binding energy. All the system nanomaterials show semi-conductor behaviour. These compounds are ESR inactive at room temperature but showed broad peaks at liquid nitrogen temperature due to spin-orbit coupling, arising due to paramagnetic $Nd^{+3}$ ions.

### *Conflict of Interests*

The authors declare that they have no conflicts of interests.

## 5. REFERENCES

1. Chavez-Guerrero L, Medina-Lott B, Cienfugos RF, Garza-Navarro MA, et al. *J. rare earth*, 2015; **33(3)**:277-281.
2. Peña MA, Fierro JLG. *Chem. Rev.*, 2001; **101(7)**:1981-2018.
3. Assirey EAR. *Saudi Pharm. J.*, 2019; **27(6)**:817-829.
4. Shah AA, Ahmad S, Azam A. *J. Magn. Magn. Mater.*, 2020; **494**:165812.
5. Ghasdi M, Alamdari H. *Sens. Actuators B Chem.*, 2010; **148**:478-485.

6. Capon F, Boileau A, Carteret C, Martin N, et al. *J. Appld. Phys.*, 2013; **114**:113510.
7. Carneiro JSA, Williams J, Gryko A, Herrera LP, et al. *ACS Catal.,* 2020; **10(1)**:516-527.
8. Gildo-Ortiz L, Guillen-Bonilla H, Salazar JS, Reyes-Gomez J, et al. *J. Nanomater.*, 2014; **8**:164380.
9. Yan JQ, Zhou JS, Goodenough JB. *Phys. Rev. B69*, 2004; 134409.
10. Thakur R. Srivastava A, Thakur R, Gaur NR. *J. Alloy. Compds.,* 2012; **516**:58-64.
11. Tepech-Carrillo I, Escobed-Morales A, Perez-Centeno A, Chico-Anota E, et al. *J. Nanomater.*, 2016; 6917950.
12. Ateia EE, Arman MM, Morsy M. *Appld. Phy. A,* 2019; **125**:883.
13. Fierro JLG. *Catal. Today*, 1990; **8**:153-174.
14. Shimizu T. Chem. Lett., 1980; **9(1)**:1-4.
15. Garin YF, Simonot L, Maire G. *Appl. Catal. B*, 1997; **11(2)**:167-179.
16. Vaz T, Salker AV. *J. Mater. Sci. Eng. B.,* 2007; **143**:81-84.
17. Abdel-Latif IA, Rahman MM, Khan SB. *Results Phys.*, 2018; **8**:578-583.
18. Garcia J, Beltran D, Sapina F, Sanches MJ. *J. Alloy. Compds.,* 1992; **188**:170-173.
19. Agarwal D, Goswam SH. *React. Kinet. Catal. Lett.,* 1994; **53(2):**441-449.
20. Brown G, Kirkby CJ, Thorp JS. *J. Mater. Sc.*, 1974; **9(1)**:65-73.
21. Baiker A, Marti PE, Keusch P, Reller A. *J. Catal.*, 1994; **146**:268-276.
22. Futai M, Yonghua C, Louhui. *React. Kinet. Catal. Lett.,* 1986; **31(1)**:47-53.